Hydroclimatic impacts of '8.2-ka event' in western Indo-Pacific Warm Pool

Yama Dixit (ydixit@iitd.ac.in)
IIT Delhi

Stephen Chua
https://orcid.org/0000-0001-6089-6097

Yu Ting Yan
Nanyang Technological University

Adam Switzer
Nanyang Technological University https://orcid.org/0000-0002-4352-7852

Article

Keywords:

Posted Date: May 12th, 2022

DOI: https://doi.org/10.21203/rs.3.rs-1611443/v1

Abstract

The most prominent abrupt climate event during the Holocene, the '8.2 ka event', was characterized by severe cooling at high northern latitudes causing diverse hydroclimate shifts globally. To date, a precise understanding of the hydroclimate response of the Indo-Pacific Warm Pool (IPWP) region to abrupt climate changes in the North Atlantic around 8.2 ka remains elusive. Here we present a high-resolution stable carbon isotope record on foraminifera species *Asterorotalia pulchella* and sediment characteristics of a marine sediment core from the Kallang River Basin, Singapore. Foraminifer stable isotope data in concert with sedimentological proxies provide coherent evidence of weakened rainfall for ~ 180 years in the western tropical Indo-Pacific region from ~ 8.14 ka to 7.96 ka BP. A robust age model suggests that the timing of the onset of reduced convective activity in the western IPWP region lags the cooling in the North Atlantic and the synchronous droughts in the Asian and Indian monsoon regions, by ~ 100years possibly implying a north-south signal propagation via oceanic route that operates on centennial scales. The termination of the '8.2 ka event', however may have occurred near synchronously between high and low tropical regions at ~ 7.96ka BP possibly linked via both atmospheric and oceanic processes.

Introduction

Abrupt short-term climate anomalies that punctuated the otherwise stable Holocene climate have drawn considerable attention from the paleoclimate community in the past few decades [1–3]. Abrupt climate events during the Holocene also had associated cultural impacts [4–8] and are therefore crucial to examine as they may provide essential information about the climate system's sensitivity to future perturbations [9]. The most prominent of the abrupt climate anomalies during the Holocene occurred around 8.2 calendar kiloyears before present (ka BP) from the perspective of Greenland temperature change [10,11]. Greenland temperature dropped by 3°C and methane concentrations declined by 80 ppbv, suggesting a significant change in the hydrologic cycle [12]. It is now widely accepted that the drainage of meltwater from the proglacial Laurentide lakes (lakes Agassiz and Ojibway) and icesheets around 8.5 ka BP into the Hudson Bay probably caused perturbations in the North Atlantic thermohaline circulation [13,14] and slowed the Atlantic Meridional Overturning Circulation (AMOC) [15]. Now several climate model experiments demonstrate the linkage between freshwater forcing and ensuing climate change globally [16–18]. The impacts of AMOC slowing was observed in the proxy records globally, for example, cave speleothems in Oman, Yemen, China and Brazil [19,20]; marine records in the Arabian Sea [8,21]; lake sequences in northwestern India [22,23] and tropical Africa (Gasse, 2000) and the Tibetan Plateau [24]; pollen records from the Mediterranean and east Asia [25,26]; ice cores from eastern Africa [27]. Owing to its widespread evidence [28,29], it is suggested that for the Early–Middle Holocene Boundary, the '8.2 ka event' constitutes a stratigraphic marker of near global significance, now formally known as the Northgrippian [30].

The '8.2 ka event' globally is well-documented by consistent evidence from multiple sites which are robust enough for the model simulations to reproduce them [29,31]. Although the '8.2 ka event' involved smaller, shorter-lived, and less areally extensive climatic anomalies than those associated with older

events such as the Younger Dryas cold interval or Heinrich stadials, nonetheless, this event punctuated early Holocene conditions that are inferred to be similar to or even warmer than today and therefore such events can serve as a useful benchmark to understand the processes involved by anthropogenic forcing in the future, and may provide useful estimates of limits on the magnitude of climate changes possible in the future [29]. However, there is a lot of ambiguity surrounding the occurrence and nature of 8.2 ka climate anomaly in the northern hemisphere tropics with some studies supporting drying in specific regions, some regions recording a double plunging structure [20] of climate drying and others arguing that the duration of these anomalies were too long or started earlier than the North Atlantic cooling, to be attributed simply to the actual '8.2 ka event' [29,32]. In particular, the effect of 8.2 ka North Atlantic cooling on the hydroclimatic variability in the Indo-Pacific Warm Pool (IPWP) region remains ambiguous [33].

The IPWP is known as the largest area of warm sea surface temperatures with the highest rainfall on Earth. It is also the largest source of atmospheric water vapor and latent heat and therefore drives the global atmospheric and hydrologic circulation [34]. The complex climatic system of the IPWP is controlled by large-scale phenomena such as the seasonal migration of the Intertropical Convergence Zone (ITCZ) which causes the northwest and southeast monsoon circulation in the region as well as the tropical Pacific climate phenomena, the Indian Ocean Dipole in the west and the El Niño-Southern Oscillation operating to the east. In addition to interactions of these climate phenomena, their influence varies across the region due to island topography and ocean–atmosphere fluxes, which are mainly imposed by sea-surface temperature (SST) variability [35]. Because the IPWP lies at the intersection of such complex zonal and meridional hydrological processes, it is important to have a clearer understanding of how this region responded to abrupt climate changes such as the '8.2 ka event' in the past.

Here we present high-resolution (sub centennial) stable carbon isotope record of carbonate shells of benthic foraminifer species *Asterorotalia trispinosa* and sediment element analyses using X-ray fluorescence data from a shallow marine sediment core retrieved from Kallang River Basin, Singapore. We compare this data with a suite of regional records to examine the similarities/dissimilarities in the nature of hydroclimate variability documented in the IPWP region between 7.0–8.5 ka BP. We also analyze the timing of 8.2 ka-climate anomaly in the IPWP region in comparison with the evidence from the North Atlantic and the Asian- Indian monsoon regions with the aim to discuss the possible controls associated with the propagation of the '8.2 ka event'. Our results discuss the possible causes to which the intra IPWP climate variability be attributed to and also the lead/lags observed in proxy records.

Kallang River Basin, Singapore

The Kallang River Basin (KRB) is located on the southern coast of Singapore (Fig. 1). This fluvio-deltaic system is predominantly made of late Quaternary sediments deposited during periods of relatively high sea levels during the present and last interglacials [36]. The coring site at Marina South, is reclaimed land that was previously a zone of shallow marine sedimentation. A continuous sediment core MS-BH01B (1.27266° N, 103.8653° E, ~ 38.5m length obtained through geotechnical rotary drilling and hydraulic piston coring, which allowed for > 90% of sediment recovery [36]. The upper ~ 12 m was identified during

wash-boring as modern fill material and discarded. The Holocene stratigraphy comprise early Holocene transgressive peats (~ 9.5 ka BP) which is succeeded by marine muds and eventually littoral/tidal silty sand deposited by ~ 7.2 ka BP. The period between 8.6 and 7.0 ka BP is well constrained by 9 AMS ^{14}C ages ranging from 7.19 ± 0.24 ka BP to 8.68 ± 0.57 ka BP. Well-preserved benthic foraminifera shells appear following the transgressive peats at ~ 8.5 ka BP, which marks the beginning of the marine unit at the study site [37]. We focus on this Holocene marine unit from 8.6 to 7.0 ka BP to study the '8.2 ka event' in the region.

Singapore experiences an equatorial type climate with rains throughout the year, with a relative minimum in June–July–August and maximum during the northern hemisphere winter from November- January with an average precipitation of ~ 250mm (Fig. 1). Rainfall, temperature and humidity are typically high year-round, and is shaped by alternating north-easterly winds associated with circulation patterns of the austral summer monsoon (November – March) and southeasterly trades that form during the boreal summer southwest monsoon (June – September) seasons, as well as local convective systems.

Results

The KRB's MSBH01B sediment core provides a high-resolution paleoclimate history from 8.5 to 7.0 ka BP. The resolution for 8.5 to 8.10 ka BP and from 7.96 to 7.50 ka BP is on average one $d^{13}C$ measurement per 40 years and 33 years for the respective interval – this was undertaken to obtain a sub-centennial scale resolution of climate variability. To determine the exact timing and structure of abrupt peaks in $d^{13}C$ values and XRF element (Al/Si and K/Al), the period from 8.14 to 7.96 ka BP was sampled and $d^{13}C$ were measured at approximately decadal scale resolution. The $d^{13}C$ values generally show a linear increasing trend across the entire period between 8.5 and 7.0 ka BP with an average of -2.63 ‰ between 8.5 and 8.1 ka BP and peak values of ~-1.77 ‰ between 8.14 and 7.96 ka BP and ~1.5 ‰ between 7.96 and 7.0 ka BP. The Al/Si and K/Al ratios have average values of 0.12 and 5.31 before and 0.14 and 3.16 respectively after the peak event. The peak drying event has an average value of 0.11 and 11.5 values for Al/Si and K/Al respectively between 8.1 and 7.96 ka BP.

Interpretation of proxy indicators

Salinity is a major governing factor on *A. pulchella* occurrence, with optimum salinity range from ~31 to 33 psu. Rao et al., (2005) reported high total abundances (live+fossil) of *A. pulchella* throughout the year, though the species was most abundant in January when the salinity was lowest (31–32 psu) and least abundant in April when the salinity was highest (34–35 psu). Stable isotopic of modern surface and subsurface samples of *A. pulchella* demonstrate that it can be used as a good candidate for paleoclimate reconstructions for the Indo–Pacific region [39]. Oxygen isotopes of foraminifer shells is controlled by the regional temperatures and the isotopic composition of the water in which the shell calcified [40], which in the case of marginal-marine/sub-tidal environments is dependent on the influx of freshwater (precipitation/evaporation or glacial melt), hence making the interpretation complex. In marginal-marine

or sub-tidal estuarine settings, the $d^{13}C$ of benthic foraminifera as a proxy of paleoproductivity/ rainfall is suggested to be more reliable than oxygen isotopes for paleoclimatic inferences [41]. The carbon isotope composition ($d^{13}C$) of dissolved inorganic carbon (DIC) which is taken up by foraminifera to form carbonate shells reflect the carbon sources in the coastal region, in particular between C3 and C4 vegetation i.e. the relative input from terrestrial (through precipitation/river runoff) and marine (marine organic matter) derived carbon ~−27‰ and ~−21‰ respectively. Such that high (low) $d^{13}C$ values thus indicate decreased (increased) input of terrestrially-derived carbon at the study site.

Selection of weathering proxies for this study was based on the understanding of the palaeohydrology and source rock mineralogy of Singapore. A previous attempt at paleochannel mapping suggest several tributaries originating predominantly from the granitic exposures and hills in central Singapore (Mote et al., 2009). Field observations reveal rapid weathering and decomposition of surficial granite forming a deep residual soil profile in the region [42,43]. The primary product of chemical weathering of granite in hot and humid tropical climates is kaolinite ($Al_2Si_2O_5(OH)_4$), a high-alumina clay which is readily remobilized [44] and flushed into fluvial channels during periods of high rainfall. Aluminium to silica (Al/Si) ratio in the bulk sediment therefore reflects the extent of chemical weathering to unweathered base rock [45]. We therefore use Al/Si as a proxy for chemical weathering as Al is normalized against other siliceous sources (e.g. quartz sand).

Both potassium (K) and aluminium (Al) occur in the clay minerals as weathering products. Potassium occurs chiefly in illite while aluminium is abundant in all clay minerals [46]. Illite is generally a weathering product in temperate to arid climatic conditions that support strong physical weathering and weak chemical weathering and kaolinite is typically a product of chemical weathering in tropical, humid climates [46,47]. Therefore K/Al is a physical to chemical weathering proxy reflecting the abundance of illite relative to kaolinite respectively. Since the bulk sediment is primarily made of clay minerals, a decrease (increase) in K/Al of the bulk sediment would indicate a decrease (increase) in illite content and an increase (decrease) in kaolinite content which in turn indicates strengthened (weak) chemical weathering owing to high (low) rainfall. Taken together, high K/Al and low Al/Si indicate decreased chemical weathering and in turn climate deterioration.

Discussion

Hydroclimate changes in the western tropical warm pool

The general long term Kallang basin $\delta^{13}C$ record follows the summer insolation at equator [48] suggesting a relatively decreasing productivity across 8.5–7.2 ka BP owing to the lower terrestrially-derived carbon brought by Kallang river runoff. For the interval under consideration in this study, the peak productivity or high rainfall period occurs between 8.5 to 8.12 ka BP (Fig. 2). This is in line with most tropical palaeo-precipitation records from north of the Equator that contain maxima in the range 10.0–8.0 ka BP [49,50]. In Southeast Asia, early Holocene were marked by submersion of large parts of the shallow landscapes in

the Sunda Shelf and northern South China Sea [51], as well as the incised channels on the continental shelves including those near Singapore. During the early Holocene, the Singapore Strait opened and ocean circulation patterns altered [52,53]. The flooding of the Sunda Shelf also contributed to increasing the quantity and intensity of moisture transport from the oceans to continents [54,55]. Such changes in both sea level and climate likely led to increased fluvial discharge from small rivers, such as Kallang and rapid infilling of the incised channels and seabed of the upper continental shelves throughout the Holocene.[53,56].

An abrupt peak in $\delta^{13}C$ of foraminifera at ~ 8.14 ka BP suggest decreased contribution of the terrestrial organic matter via the Kallang River runoff at the study site implying a weakened convective activity in the region. This is followed closely by a period of diminished chemical weathering beginning at ~ 8.05 ka BP, inferred from high K/Al values suggesting weak chemical weathering and beginning of climate deterioration (less humid conditions) in the region. The other weathering proxy Al/Si also show a lower value during this period indicating decreased kaolinite (chemical weathering product) as compared to unweathered siliceous base rock, which in turn indicates weakened chemical weathering due to lower rainfall in the region. The century scale lag in timing of the productivity/ rainfall changes (inferred from $\delta^{13}C$) and the chemical weathering (inferred from K/Al and Al/Si) presumably stems from the time taken for the silicate rocks to weather into clays and the vegetation proxies are generally believed to have responded promptly to abrupt climate events [26]. Our $\delta^{13}C$ and sediment proxy records suggest that an abrupt drying event began at 8.14 ka and ended at ~ 7.96 ka BP, lasting for about 180 years.

Regional Evidence Of The ‘8.2 Ka Event’

Owing to the high sedimentation rate (~ 4.4 mm/yr) in KRB cores, it is possible to examine the timing and nature of the ‘8.2 ka event’ in detail in this region making this an invaluable and unique archive to study up to sub-centennial changes when sampled every centimeter. This is rare in marine sediment cores which are typically characterized by lower sedimentation rates, contributing to difficulties in collating results from other regional high-resolution archives (e.g. speleothems). In the IPWP region, the discordance between the type and resolution of marine and terrestrial (speleothem, corals and lacustrine) records is one of the several reasons that climate inferences are often contradictory [33]. The ‘8.2 ka event’ in the IPWP region is rather poorly documented and the differences in timing of drying between paleoclimate records in the IPWP region mainly stems from (1) different monsoon systems/ moisture sources affecting the region; (2) inadequate age control and differing sampling resolution; and (3) complex topography of the region. We discuss the prominent relatively high-resolution records from the IPWP region that have documented an 8.2 ka signal with respect to the KRB records in this section.

The timing of drying between 8.14 and 7.96 ka BP recorded in the KRB cores is coincident with the drying peak recorded in Gunung Buda cave in Borneo [57]. Both these records document changes in the local convective rainfall as compared to the variability in zonal and meridional processes such as the monsoon systems plying to the west (Indian monsoon), north (Asian monsoon), or south (Indonesian-

Australian monsoon) of the region. Mohtadi et al., (2014) used surface-dwelling planktonic foraminifer *Globigerinoides ruber* $\delta^{18}O$ to reconstruct variations in salinity from three marine sedimentary records off Sumatra spanning 45ka and identified '8.2 ka event' along with past Heinrich events as dry periods in the northern Indian Ocean realm linked with the North Atlantic cold spells. A close inspection of these Sumatra marine records reveals a difference in timing of the 8.2 drying: 8.4–8.2 ka BP (in SO189-39KL), 8.3–8.1 ka (in SO189-144KL) and the northernmost core SO-189-119KL showing no drying at all across 8.5- 7.0 ka BP interval (Fig. 3). The inconsistency in the timing of drying between these three northern Sumatra cores can probably be attributed to the inadequate age control and sampling resolution for each of the cores (see Fig. 3). Another prominent study from the Sumatran island is from Tangga Cave speleothems which document a drying peak between 8.4 to 8.1 ka BP, centered at ~ 8.25 ka BP [33]. Both of the marine cores off Sumatra as well as the Tangga cave speleothems seem to have a fairly similar timing of drying centered at ~ 8.25 ka BP, which is also coincident with the drying in the Indian monsoon regions (Fig. 4d). However, the timing of drying in the marine cores off Sumatra and Tannga Cave speleothems leads the drying in the Kallang core and Borneo speleothem records by about 100 years. Together, Sumatran marine and speleothem records portray a broad reduction in the hydrological activity around 8.25 ka BP in western Sumatra mostly influenced by the equatorial Indian Ocean dynamics, which also plays a crucial role in the Indian summer monsoon variability. On the other hand, Liang Luar cave speleothems from Flores, Indonesia which record the Australian-Indonesian monsoon variability, document no distinct drying around 8.2 ka BP and instead just follows the austral summer insolation with increasing rainfall from early to middle Holocene [58].

Overall, the KRB proxy records provide an unequivocal evidence for weakening in the local convective rainfall in the western IPWP between 8.14 and 7.96 ka BP associated with the 8.2 ka cooling in the North Atlantic. The KRB record thus adds to the growing body of evidence of the impact of the cooling in the high latitudes on the regional hydroclimate in the tropical oceans during the Holocene.

Comparison With North Atlantic And Indian-asian Monsoon Records

It is clear that the 8.2 ka cold event in the North Atlantic was rapidly communicated through the ocean by an AMOC slowdown and through changes in atmospheric circulation that caused climate anomalies worldwide [1,13]. Therefore the magnitude of temporal offsets and geographic reach can only be explained through a combination of atmospheric (faster, on decadal scale) and oceanic (slower, centennial scale) processes [59–61]. The exact timing of the early Holocene meltwater pulse has been dated to 8.47 ± 0.3 kyr BP (1σ) (Barber et al., 1999), with the onset of the sharp cooling in the Greenland ice cores at ~ 8.25 ka BP (Fig. 4) [62,63]. The timing of cooling centered at ~ 8.2 ka BP in Greenland ice cores is synchronous to weakening of the Indian and Asian monsoon in well dated prominent speleothem records from Oman and China (Fig. 4). The widely accepted mechanism for the coincident timing of the climate anomalies in the North Atlantic and the monsoon regions is the signal propagation both via ocean and atmospheric energy

transport. Decreased heat transport through oceans tend to shift the ITCZ southwards [20]. Model simulations demonstrate that the ocean meridional overturning circulation contributes significantly to the hemispheric asymmetry in tropical rainfall by transporting heat from the Southern to the Northern Hemisphere, and thereby positioning the ITCZ northward, regardless of whether continents are present or not [64]. Therefore a consequence of North Atlantic cooling related to the reduced strength of the meridional overturning circulation is more southwardly located ITCZ and a decline of monsoon rainfall [64]. The role of cross equatorial energy transport via atmosphere controlling the ITCZ position is also suggested such that the position of ITCZ tends to shift southward as the northward atmospheric energy transport across the equator strengthens in response to a northern high-latitude cooling [65–67]. Furthermore, the impact of change in Eurasian ice cover on the position of ITCZ is suggested via reinforcement of boreal cooling [68]. Thus a combination of atmospheric and oceanic processes linked to the North Atlantic cooling displaced the mean latitudinal position of the ITCZ to the south in phase with the Northern Hemisphere cooling. This north to south directionality, via the atmosphere and oceanic route, of signal propagation also corroborates with the hypothesis proposed for the Younger Dryas and older cold periods of the Dansgaard–Oeschger cycles [60,69].

Within the uncertainty of 14C dated age model, the timing of the onset of drying at 8.14 ka BP observed in KRB core, however, lags the timing of the onset of the North Atlantic cooling and monsoon weakening by ~ 100 years. The termination of the ‘8.2 ka event’ at ~ 7.96 ka BP in Kallang records, however is synchronous with the North Atlantic and the monsoon regions (Fig. 4).

A variety of mechanisms have been proposed to explain the signal propagation from the North Atlantic to the tropical Indo-Pacific hydroclimates for past cold events primarily via oceanic route : (1) a weakening of the rainfall system in response to regional sea surface cooling; and (2) changes in the monsoon intensity associated with a southward shift in the mean or winter position of the ITCZ or in the position of oceanic fronts [71]. Owing to the location of Singapore in the western Indo-Pacific warm ocean region, its complex climatic system is controlled by the combined influence of ITCZ migration, IOD, ENSO, all of which are mainly imposed by SST variability [35]. The northern high-latitude to low latitude directionality of cooling signal was possibly communicated to the tropical IPWP mainly through the oceanic route (on centennial scale) causing about a century scale lag. This highlights the role of oceanic processes (mainly via changes in Southern Ocean temperature) in response to the abrupt change in the AMOC strength via the bipolar seesaw [72,73]. This mechanism is consistent with the notion that convectional rainfall in the tropical warm pool region is fundamentally driven by oceanic dynamics and especially SST changes [35]. A similar hypothesis has been recently proposed for the Younger Dryas period, although the magnitude of cooling was much higher if compared to the ‘8.2 ka event’ [69]. Mohtadi et al.,[71]suggested that the response of tropical Indian ocean involved similar mechanisms for the Heinrich stadials, the Younger Dryas and the ‘8.2 ka event’, irrespective of glacial background climate states.

Unlike the Younger Dryas termination which is believed to have initiated in the tropical Pacific region and propagated to high latitudes, suggesting a tropics to North Atlantic–Asian Monsoon-Westerlies

directionality of climatic recovery [69], the termination of the '8.2 ka event' have a synchronous timing across the tropical Pacific- Indian/Asian monsoon – North Atlantic [19,21,70]. Modeling simulations provide a possible explanation for the centennial scale duration and synchronous termination of the '8.2 ka event'. The 8.2 ka event demonstrated the existence of an additional equilibrium climate state primarily controlled by the freshwater pulse causing reduced North Atlantic Deep Water formation, following which when the meltwater runoff eventually waned, the initial circulation pattern was rapidly restored near synchronously as the cold phase ended as seen in anomalies worldwide synchronously[18,74].

Summary And Conclusions

It is imperative to analyse the cold event such as the '8.2 ka event' to understand the impacts of future freshening of the North Atlantic forced by anthropogenic global warming. Most 8.2 ka climate anomalies documented in the existing paleoclimate records in mid-low-latitude systems suggest the downstream impacts of a meltwater pulse into the North Atlantic and its associated sharp cooling event. Rohling et al.,[75] suggested that such a mechanism cannot be held responsible for the climate anomaly of longer duration and/or early onset of climate deterioration well before the North Atlantic cold event and careful consideration needs to be given while evaluating climate anomalies around '8.2 ka event' and establishing their causal mechanism.

Our high resolution KRB record adds to a growing body of evidence of the response of regional hydroclimate changes in the tropical IPWP region to the North Atlantic forcing coincident with the '8.2 ka event'. Owing to the location of the sediment core, the KRB provide independent records of local convective rainfall of the western IPWP and a clear evidence of a drying event that lasted for about 180 years from 8.14–7.96 ka BP. We suggest that this drying event was the tropical ocean response to the '8.2 ka cold event' in the North Atlantic. The timing of the onset of drying in our record lags the North Atlantic cooling and concomitant drying in monsoon regions by about a century, which is possibly due to the time taken for the redistribution of heat via oceanic processes.

Our proposed mechanism explaining the timing and mechanism of 8.2 ka signal propagation is based on high-resolution KRB proxy records in conjunction with previously published modeling and proxy studies. Nonetheless the causal sequence and mechanism between tropics and the North Atlantic still remains a challenging issue for modeling approaches and therefore more proxy records with precise chronology and spatial distribution spanning the entire complex IPWP are valuable for future model simulations.

Materials And Methods

Stable isotope ratios of *Asterorotalia pulchella*

We used benthic foraminifer species *Asterorotalia pulchella* for stable carbon and oxygen isotopic analysis. *A. pulchella* is a benthic epifaunal foraminifera found to be endemic in South Asia. Previous studies conducted along other inner shelves environment such as Moutama Bay, Muthupet Lagoon and

Pahang River estuary show that it is a dominant species found in marginal marine environments [76–79]. This species is generally found in areas where water depth is low with fine-grained silty to muddy substrate. A. pulchella is also able to tolerate a wider range of salinity, from 34 to as low as 29 psu, making it more euryhaline than other marine species [39,80]. Its ability to tolerate a wider range of salinity makes it a suitable candidate to ensure that this species is present throughout the period of interest where freshwater influx is expected to vary. Previously, Panchang & Nigam (2012) also demonstrated that stable isotopes of A. pulchella carbonate shells can be used for paleoclimate reconstructions for the Indo-Pacific region where this species is found to be prevalent in marginal marine environments.

Approximately 5–15 individual tests were picked for each measurement and analysed using a Thermo Delta V isotope ratio mass spectrometer coupled with GasBench housed at the Asian School of Environment, Nanyang Technological University, Singapore. The isotopic composition of the carbonate sample was measured on the CO2 gas evolved by treatment with phosphoric acid at a constant temperature of 75°C. For all stable isotope measurements an internal working standard was used, which has been calibrated against VPDB (Vienna Pee Dee Belemnite) by using the NBS 18 and 19 standards. Consequently, all isotopic data given here are relative to the VPDB standard. Analytical standard deviation is about ± 0.06‰ for $\delta^{13}C$.

X-Ray Fluorescence (XRF) scanning

We measured the relative elemental composition of the core segments using an Avaatech micro- X-Ray Fluorescence (XRF) Core Scanner II (AVAATECH Serial No. 2) housed at the Asian School of the Environment, Nanyang Technological University. Each core surface was carefully covered with 4 µm SPEXCerti Prep Ultralene® film to avoid sample contamination and carefully smoothed using sterile plastic scrappers. All core segments were scanned at 1 cm resolution with measurement slit size at 1 x 1 cm. Generator settings of 10 kV and 30 kV settings, coupled with exposure times of 15 s and 25 s respectively, were used to measure elemental abundance counts from Aluminium (Al) to Iron (Fe). All element counts were normalized to the total count numbers to correct for drift of the XRF Core Scanner.

Age model

The age model is based on 16 accelerator mass spectrometry (AMS) ^{14}C ages ranging from 9.5 to 7.2 ka BP [37]. AMS ^{14}C dating was carried out at the Rafter Radiocarbon Laboratory at GNS Science, New Zealand. Radiocarbon ages were converted to calibrated calendar years before present (ka BP) using the calibration software CALIB 8.2 (Stuiver, et al., 2020) and the IntCal20 (Reimer et al., 2020) and Marine20 calibration curves [82]. ΔR was calculated using the *deltar* application [83] from a paired *in situ* bivalve-wood sample in core MSBH01B [37].

The age-depth model was produced using BChron (Parnell, 2020), an open source R package utilising a Bayesian statistical approach, which provides uncertainties and increases robustness of the age model,

for chronological reconstruction. Here, 1050 age-depth realizations were obtained to estimate the median age and 95% confidence intervals at 1 cm resolution.

Declarations

Acknowledgements

This research was supported by the Earth Observatory of Singapore (EOS) grants M4430132.B50-2014 (Singapore Quaternary Geology), M4430139.B50-2015 (Singapore Holocene Sea Level), M4430188.B50-2016 (Singapore Drilling Project), M4430245.B50-2017 and M4430245.B50-2018 (Kallang Basin Project) and 04MNS001985A620OOE01 (Maritime Continent Project). This research was supported by the EOS via its funding from the National Research Foundation Singapore and the Singapore Ministry of Education under the Research Centres of Excellence initiative. This work comprises EOS contribution number 340. The authors thank the Director of the Earth Observatory of Singapore, Prof. Ben Horton for his support and Dr. Huixian Chen for help with foraminifera identification and extraction.

References

1. Alley, R. B. *et al.* Holocene climatic instability: A prominent, widespread event 8200 yr ago. *Geology* **25**, 483–486 (1997).

2. Wanner, H., Solomina, O., Grosjean, M., Ritz, S. P. & Jetel, M. Structure and origin of Holocene cold events. *Quat. Sci. Rev.* **30**, 3109–3123 (2011).

3. Mayewski, P. A. *et al.* Holocene climate variability. *Quat. Res.* **62**, 243–255 (2004).

4. Dixit, Y., Hodell, D. A. & Petrie, C. A. Abrupt weakening of the summer monsoon in northwest India ~4100 yr ago. *Geology* **42**, 339–342 (2014).

5. Dixit, Y. *et al.* Intensified summer monsoon and the urbanization of Indus Civilization in northwest India. *Sci. Rep.* **8**, (2018).

6. Petrie, C. A. *et al.* Adaptation to Variable Environments, Resilience to Climate Change: Investigating Land, Water and Settlement in Indus Northwest India. *Curr. Anthropol.* **58**, 0 (2017).

7. Roffet-Salque, M. *et al.* Evidence for the impact of the 8.2-kyBP climate event on Near Eastern early farmers. *Proc. Natl. Acad. Sci.* **115**, 8705 LP – 8709 (2018).

8. Staubwasser, M. & Weiss, H. Holocene Climate and Cultural Evolution in Late Prehistoric–Early Historic West Asia. *Quat. Res.* **66**, 372–387 (2006).

9. Curry, R., Dickson, B. & Yashayaev, I. A change in the freshwater balance of the Atlantic Ocean over the past four decades. *Nature* **426**, 826–829 (2003).

10. Thomas, E. R. *et al.* The 8.2 ka event from Greenland ice cores. *Quat. Sci. Rev.* **26**, 70–81 (2007).

11. Alley, R. B. & Ágústsdóttir, A. M. The 8k event: cause and consequences of a major Holocene abrupt climate change. *Quat. Sci. Rev.* **24**, 1123–1149 (2005).

12. Kobashi, T., Severinghaus, J. P., Brook, E. J., Barnola, J.-M. & Grachev, A. M. Precise timing and characterization of abrupt climate change 8200 years ago from air trapped in polar ice. *Quat. Sci. Rev.* **26**, 1212–1222 (2007).

13. Barber, D. C. *et al.* Forcing of the cold event of 8,200 years ago by catastrophic drainage of Laurentide lakes. *Nature* **400**, 344–348 (1999).

14. Wagner, A. J., Morrill, C., Otto-Bliesner, B. L., Rosenbloom, N. & Watkins, K. R. Model support for forcing of the 8.2 ka event by meltwater from the Hudson Bay ice dome. *Clim. Dyn.* **41**, 2855–2873 (2013).

15. Kleiven, H. K. F. *et al.* Reduced North Atlantic deep water coeval with the glacial Lake Agassiz freshwater outburst. *Science (80-.).* **319**, 60–64 (2008).

16. LeGrande, A. N. *et al.* Consistent simulations of multiple proxy responses to an abrupt climate change event. *Proc. Natl. Acad. Sci.* **103**, 837–842 (2006).

17. Wiersma, A. P. & Renssen, H. Model–data comparison for the 8.2 ka BP event: confirmation of a forcing mechanism by catastrophic drainage of Laurentide Lakes. *Quat. Sci. Rev.* **25**, 63–88 (2006).

18. Matero, I. S. O., Gregoire, L. J., Ivanovic, R. F., Tindall, J. C. & Haywood, A. M. The 8.2 ka cooling event caused by Laurentide ice saddle collapse. *Earth Planet. Sci. Lett.* **473**, 205–214 (2017).

19. Fleitmann, D. *et al.* Holocene Forcing of the Indian Monsoon Recorded in a Stalagmite from Southern Oman. *Science (80-.).* **300**, 1737 (2003).

20. Cheng, H. *et al.* Timing and structure of the 8.2 kyr BP event inferred from δ18O records of stalagmites from China, Oman, and Brazil. *Geology* **37**, 1007–1010 (2009).

21. Gupta, A. K., Anderson, D. M. & Overpeck, J. T. Abrupt changes in the Asian southwest monsoon during the Holocene and their links to the North Atlantic Ocean. *Nature* **421**, 354–357 (2003).

22. Dixit, Y. Regional character of the “global monsoon”:Paleoclimate insights from Northwest Indian lacustrine sediments. *Oceanography* **33**, (2020).

23. Dixit, Y., Hodell, D. A., Sinha, R. & Petrie, C. A. Abrupt weakening of the Indian summer monsoon at 8.2 kyr B.P. *Earth Planet. Sci. Lett.* **391**, 16–23 (2014).

24. Mischke, S. & Zhang, C. Holocene cold events on the Tibetan Plateau. *Glob. Planet. Change* **72**, 155–163 (2010).

25. Peyron, O. *et al.* Precipitation changes in the Mediterranean basin during the Holocene from terrestrial and marine pollen records: a model–data comparison. *Clim. Past* **13**, 249–265 (2017).

26. Park, J. *et al.* The 8.2 ka cooling event in coastal East Asia: High-resolution pollen evidence from southwestern Korea. *Sci. Rep.* **8**, 12423 (2018).

27. Thompson, L. G. *et al.* Kilimanjaro ice core records: evidence of Holocene climate change in tropical Africa. *Science (80-.).* **298**, 589–593 (2002).

28. Morrill, C. & Jacobsen, R. How widespread were climate anomalies 8200 years ago? *Geophys. Res. Lett.* **32**, (2005).

29. Morrill, C. *et al.* Proxy benchmarks for intercomparison of 8.2 ka simulations. *Clim. Past* **9**, (2013).

30. Walker, M. *et al.* Subdividing the Holocene Series/Epoch: formalization of stages/ages and subseries/subepochs, and designation of GSSPs and auxiliary stratotypes. *J. Quat. Sci.* **34**, 173–186 (2019).

31. Alley, R. B. *et al.* Proxy benchmarks for intercomparison of 8.2 ka simulations. *Nature* **9**, 205–214 (2013).

32. Voarintsoa, N. R. G. *et al.* Investigating the 8.2 ka event in northwestern Madagascar: Insight from data–model comparisons. *Quat. Sci. Rev.* **204**, 172–186 (2019).

33. Wurtzel, J. B. *et al.* Tropical Indo-Pacific hydroclimate response to North Atlantic forcing during the last deglaciation as recorded by a speleothem from Sumatra, Indonesia. *Earth Planet. Sci. Lett.* **492**, 264–278 (2018).

34. De Deckker, P. The Indo-Pacific Warm Pool: critical to world oceanography and world climate. *Geosci. Lett.* **3**, 20 (2016).

35. Aldrian, E. & Dwi Susanto, R. Identification of three dominant rainfall regions within Indonesia and their relationship to sea surface temperature. *Int. J. Climatol. A J. R. Meteorol. Soc.* **23**, 1435–1452 (2003).

36. Chua, S. *et al.* A new Quaternary Stratigraphy of the Kallang River Basin, Singapore: Implications for Urban Development and Geotechnical Engineering in Singapore. *J. Asian Earth Sci.* 104430 (2020).

37. Chua, S. Quaternary palaeoenvironments of the Kallang River Basin, Singapore. (Nanyang Technological University, 2019). doi:https://doi.org/10.32657%2F10220%2F48572.

38. Rao, P. S., Ramaswamy, V. & Thwin, S. Sediment texture, distribution and transport on the Ayeyarwady continental shelf, Andaman Sea. *Mar. Geol.* **216**, 239–247 (2005).

39. Panchang, R. & Nigam, R. High resolution climatic records of the past~ 489 years from Central Asia as derived from benthic foraminiferal species, Asterorotalia trispinosa. *Mar. Geol.* **307**, 88–104 (2012).

40. Shackleton, N. J. Oxygen isotopes, ice volume and sea level. *Quat. Sci. Rev.* **6**, 183–190 (1987).

41. Diz, P. *et al.* Interpretation of benthic foraminiferal stable isotopes in subtidal estuarine environments. *Biogeosciences* **6**, 2549–2560 (2009).

42. Zhao, J., Broms, B. B., Zhou, Y. & Choa, V. A study of the weathering of the Bukit Timah granite Part B: field and laboratory investigations. *Bull. Int. Assoc. Eng. Geol. l'Association Int. Géologie l'Ingénieur* **50**, 105–111 (1994).

43. Rahardjo, H., Aung, K. K., Leong, E. C. & Rezaur, R. B. Characteristics of residual soils in Singapore as formed by weathering. *Eng. Geol.* **73**, 157–169 (2004).

44. Rothwell, R. G. Twenty years of XRF core scanning marine sediments: what do geochemical proxies tell us? in *Micro-XRF Studies of Sediment Cores* 25–102 (Springer, 2015).

45. Tian, J., Xie, X., Ma, W., Jin, H. & Wang, P. X-ray fluorescence core scanning records of chemical weathering and monsoon evolution over the past 5 Myr in the southern South China Sea. *Paleoceanography* **26**, (2011).

46. Boyle, E. A. Chemical accumulation variations under the Peru Current during the past 130,000 years. *J. Geophys. Res. Ocean.* **88**, 7667–7680 (1983).

47. Yarincik, K. M., Murray, R. W. & Peterson, L. C. Climatically sensitive eolian and hemipelagic deposition in the Cariaco Basin, Venezuela, over the past 578,000 years: Results from Al/Ti and K/Al. *Paleoceanography* **15**, 210–228 (2000).

48. Berger, A. Long-Term Variations of Daily Insolation and Quaternary Climatic Changes. *J. Atmos. Sci.* **35**, 2362–2367 (1978).

49. Stott, L. *et al.* Decline of surface temperature and salinity in the western tropical Pacific Ocean in the Holocene epoch. *Nature* **431**, 56–59 (2004).

50. Haug, G. H., Hughen, K. A., Sigman, D. M., Peterson, L. C. & Röhl, U. Southward Migration of the Intertropical Convergence Zone Through the Holocene. *Science (80-.).* **293**, 1304 LP – 1308 (2001).

51. Hanebuth, T., Stattegger, K. & Grootes, P. M. Rapid flooding of the Sunda Shelf: a late-glacial sea-level record. *Science (80-.).* **288**, 1033–1035 (2000).

52. Smith, D. E., Harrison, S., Firth, C. R. & Jordan, J. T. The early Holocene sea level rise. *Quat. Sci. Rev.* **30**, 1846–1860 (2011).

53. Bird, M. I., Pang, W. C. & Lambeck, K. The age and origin of the Straits of Singapore. *Palaeogeogr. Palaeoclimatol. Palaeoecol.* **241**, 531–538 (2006).

54. Cook, C. G. & Jones, R. T. Palaeoclimate dynamics in continental Southeast Asia over the last ~30,000Calyrs BP. *Palaeogeogr. Palaeoclimatol. Palaeoecol.* **339**–**341**, 1–11 (2012).

55. Liew, P.-M., Huang, S.-Y. & Kuo, C.-M. Pollen stratigraphy, vegetation and environment of the last glacial and Holocene—A record from Toushe Basin, central Taiwan. *Quat. Int.* **147**, 16–33 (2006).

56. Zong, Y. *et al.* The role of sea-level rise, monsoonal discharge and the palaeo-landscape in the early Holocene evolution of the Pearl River delta, southern China. *Quat. Sci. Rev.* **54**, 77–88 (2012).

57. Partin, J. W., Cobb, K. M., Adkins, J. F., Clark, B. & Fernandez, D. P. Millennial-scale trends in west Pacific warm pool hydrology since the Last Glacial Maximum. *Nature* **449**, 452–455 (2007).

58. Griffiths, M. L. *et al.* Increasing Australian–Indonesian monsoon rainfall linked to early Holocene sea-level rise. *Nat. Geosci.* **2**, 636–639 (2009).

59. Fudge, T. J. *et al.* Onset of deglacial warming in West Antarctica driven by local orbital forcing. *Nature* **500**, 440 (2013).

60. Markle, B. R. *et al.* Global atmospheric teleconnections during Dansgaard–Oeschger events. *Nat. Geosci.* **10**, 36–40 (2017).

61. Buizert, C. *et al.* Abrupt ice-age shifts in southern westerly winds and Antarctic climate forced from the north. *Nature* **563**, 681–685 (2018).

62. Svensson, A. *et al.* A 60 000 year Greenland stratigraphic ice core chronology. *Clim. Past* **4**, 47–57 (2008).

63. Rasmussen, S. O. *et al.* A new Greenland ice core chronology for the last glacial termination. *J. Geophys. Res. Atmos.* **111**, (2006).

64. Frierson, D. M. W. *et al.* Contribution of ocean overturning circulation to tropical rainfall peak in the Northern Hemisphere. *Nat. Geosci.* **6**, 940–944 (2013).

65. Bischoff, T. & Schneider, T. The equatorial energy balance, ITCZ position, and double-ITCZ bifurcations. *J. Clim.* **29**, 2997–3013 (2016).

66. Kang, S. M., Frierson, D. M. W. & Held, I. M. The tropical response to extratropical thermal forcing in an idealized GCM: The importance of radiative feedbacks and convective parameterization. *J. Atmos. Sci.* **66**, 2812–2827 (2009).

67. Donohoe, A., Marshall, J., Ferreira, D., Armour, K. & McGee, D. The interannual variability of tropical precipitation and interhemispheric energy transport. *J. Clim.* **27**, 3377–3392 (2014).

68. Liu, Y.-H. *et al.* Links between the East Asian monsoon and North Atlantic climate during the 8,200 year event. *Nat. Geosci.* **6**, 117–120 (2013).

69. Cheng, H. *et al.* Timing and structure of the Younger Dryas event and its underlying climate dynamics. *Proc. Natl. Acad. Sci.* **117**, 23408 LP – 23417 (2020).

70. Wang, Y. *et al.* The Holocene Asian monsoon: links to solar changes and North Atlantic climate. *Science (80-.).* **308**, 854–857 (2005).

71. Mohtadi, M. *et al.* North Atlantic forcing of tropical Indian Ocean climate. *Nature* **509**, 76–80 (2014).

72. Broecker, W. S. Paleocean circulation during the last deglaciation: a bipolar seesaw? *Paleoceanography* **13**, 119–121 (1998).

73. Shakun, J. D. & Carlson, A. E. A global perspective on Last Glacial Maximum to Holocene climate change. *Quat. Sci. Rev.* **29**, 1801–1816 (2010).

74. Bauer, E., Ganopolski, A. & Montoya, M. Simulation of the cold climate event 8200 years ago by meltwater outburst from Lake Agassiz. *Paleoceanography* **19**, (2004).

75. Rohling, E. Centennial-scale climate cooling with a sudden cold event around 8,200 years ago. *Quat. Sci. Rev.* **26**, 172–186 (2005).

76. Ramlan, O. & Noraswana, N. F. Distribution of benthic Foraminifera in Pahang River estuary, Malaysia. *Malaysian Appl. Biol.* **44**, 1–5 (2015).

77. Saidova, K. M. Benthic foraminifera communities of the Andaman Sea (Indian Ocean). *Oceanology* **48**, 517–523 (2008).

78. Anbuselvan, N. Benthic foraminiferal distribution and biofacies in the shelf part of Bay of Bengal, east coast of India. *Mar. Biodivers.* **49**, 691–706 (2019).

79. Szarek, R., Kuhnt, W., Kawamura, H. & Kitazato, H. Distribution of recent benthic foraminifera on the Sunda Shelf (South China Sea). *Mar. Micropaleontol.* **61**, 171–195 (2006).

80. Solai, A., Gandhi, M. S. & Rao, N. R. Recent benthic foraminifera and their distribution between Tuticorin and Tiruchendur, Gulf of Mannar, south-east coast of India. *Arab. J. Geosci.* **6**, 2409–2417 (2013).

81. Reimer, P. J. *et al.* The IntCal20 northern hemisphere radiocarbon age calibration curve (0–55 cal kBP). *Radiocarbon* **62**, 725–757 (2020).

82. Heaton, T. J. *et al.* Marine20—the marine radiocarbon age calibration curve (0–55,000 cal BP). *Radiocarbon* **62**, 779–820 (2020).

83. Reimer, R. W. & Reimer, P. J. An online application for [...] R calculation. *Radiocarbon* **59**, 1623 (2017).

Figures

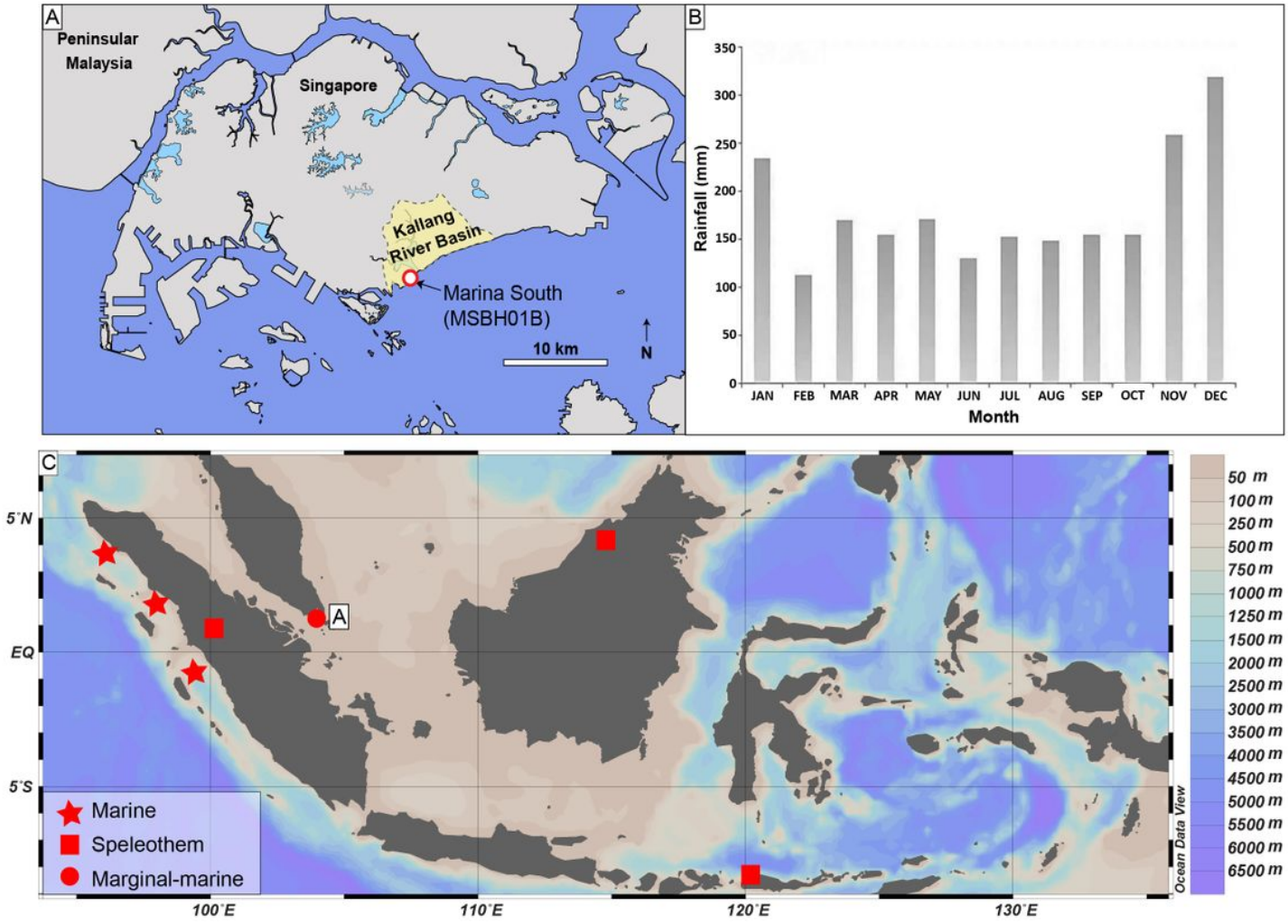

Figure 1

(a) Map of Singapore showing approximate extent of the Kallang River Basin (yellow shading); (b) Mean monthly precipitation (1981–2010) for Singapore from Changi climate station (1981-2010) Source : weather.gov.sg (accessed 10 October 2019); (c) Topographic map of the Maritime Continent with prominent published paleoclimate work used in this study marked. Red circle denotes location of the sediment core MSBH01B. Note that the current coastline is reclaimed and further seaward than during the early Holocene.

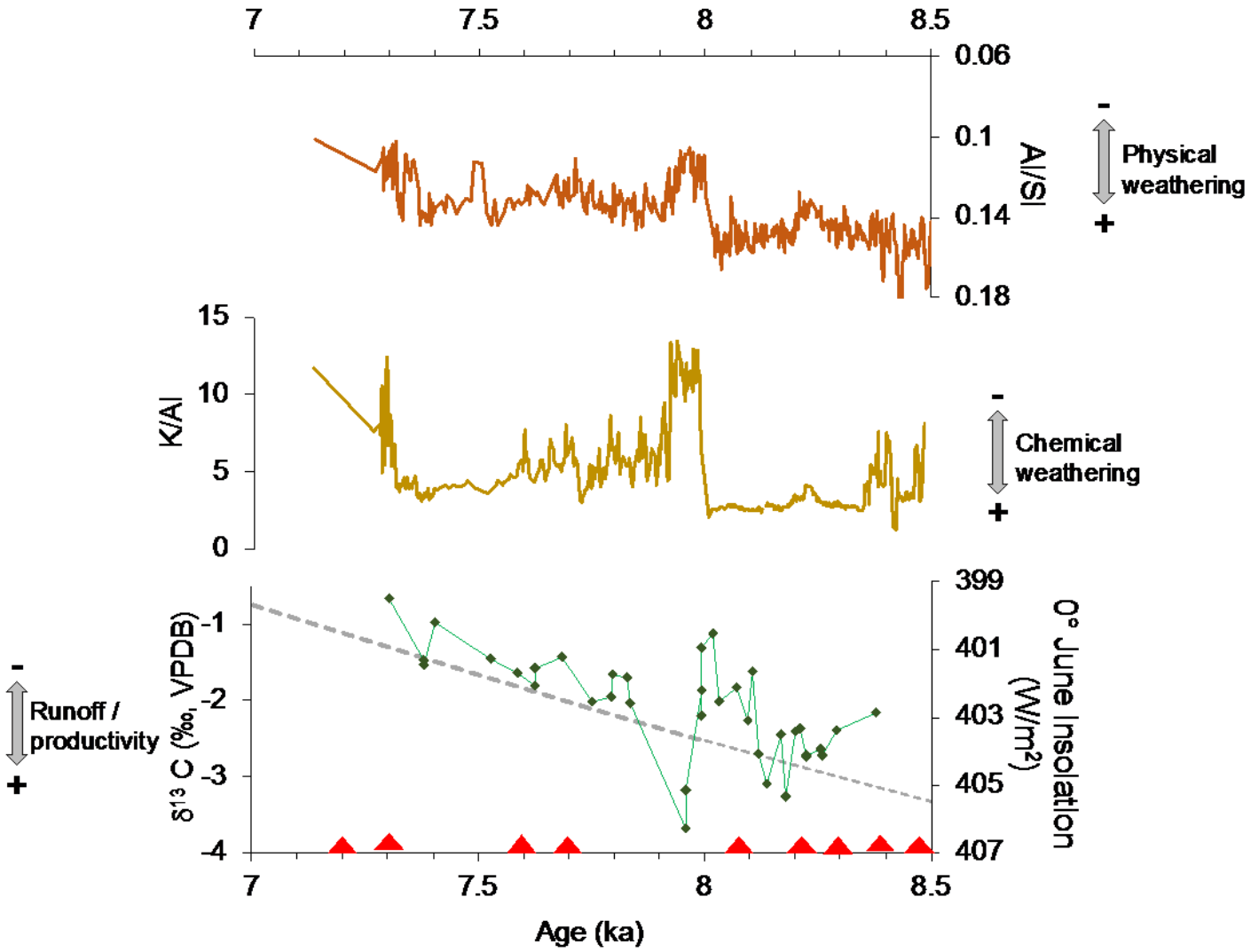

Figure 2

Results from KRB sediment core MSBH01B. Stable carbon isotopes on benthic foraminifera A. pulchella (green), summer insolation at equator in W/m^2 in grey dashed line [48] and K/Al (pale yellow) and Al/Si (orange) XRF elemental ratios on the sediment core. Note that the insolation values are plotted in reverse axis to highlight productivity (rainfall/runoff) following decreasing insolation from 8.5 to 7.0 ka BP.

Figure 3

Comparison of results from KRB core MSBH01B with other prominent paleoclimate studies from the IPWP region. (A) Speleothem d^{18}O from Tangga Cave, Sumatra (Wurtzel et al., 2018); (B) d^{18}O of foraminifera G. ruber from marine sediment cores off northwestern Sumatra (Mohtadi et al., 2014); (C) Liang Luar cave speleothem d^{18}O, Flores (Griffiths et al., 2009); (D) Gunung Buda Cave speleothem d^{18}O, Borneo (Partin et al., 2007); (E) Al/Si count , (F) K/Al counts from MSBH01B core (this study); (G) d^{13}C of benthic foraminifera A. pulchella from MSBH01B core (this study). Red triangles at the bottom denote the

^{14}C AMS dated horizons in the MSBH01B core and the red squares in other records denote the dated horizons in the 7.0-8.5 ka BP interval. Orange bar denote the ‘8.2 ka event’ observed in Kallang record from 8.14-7.96 ka BP. The dashed red line indicates the end of the drying period at ~7.95 ka BP in all the records.

Figure 4

Comparison of results from KRB core MSBH01B results with NGRIP, Asian and Indian monsoon studies. (A) Greenland NGRIP $d^{18}O$ [63]; (B) Dongge Cave $d^{18}O$, China [70]; (C) Qunf Cave speleothem $d^{18}O$ [19]; (D) %G. bulloides from Arabian Sea [21]; (E) Al/Si count , (F) K/Al counts from MSBH01B core (this study); (G) $d^{13}C$ of benthic foraminifera A. pulchella from MSBH01B core (this study). Red triangles at the bottom denote the ^{14}C AMS dated horizons in the MSBH01B core and the red squares in other records denote the dated horizons in the 7.0-8.5 ka BP interval. The orange bar denotes the drying event observed in Kallang record from 8.14-7.96 ka BP. The dashed red line indicates the beginning of the ‘8.2 ka event’ in the Greenland at ~8.25 ka BP and end of the drying period at ~7.95 ka BP in all the records.